Cohesive Zone Analysis of Crack Propagation on a Hierarchical Structured Interface

Xiaoru Wang[1], **Akihiro Nakatani**[1,*]

[1] Department of Adaptive Machine Systems, Osaka University, Suita, Osaka 565-0871, Japan

[*] Corresponding author: nakatani@ams.eng.osaka-u.ac.jp

Abstract Hierarchical ramification structures are found of superior strength during fracture. Crack propagation along cohesive zone model binding with hierarchical ramification structures is simulated to analyze the fracture process. The feature of specified bonding surface results special pattern of crack propagation. Therefor, the potential that by changing the morphology of the bonding surface may control the toughness of the material is illustrated.

Keywords Computational Mechanics, Cohesive Zone Model, Hierarchical Structure, Fracture Toughness, Criterion

1. Introduction

Some biological materials have the internal structures that exhibit superior performances in mechanical properties[1]. There are quite a few studies to investigate the fundamental mechanism of the biological systems in order to develop the artificial bio inspired materials. In this study, we focus on the the hierarchical ramification structures that contribute to high fracture toughness. The hierarchical ramification structures are often observed in many biological system. The structures appear as fractal geometries which are generated naturally via quite simple rules and they contribute to redundancy for safety of their life.

In this study, the cohesive zone model is adopted to a hierarchical structured interface and the crack propagation on the interface is studied.

First, the problem of double cantilever beam problem is solved to estimate the fundamental effect of the microstructure of interface. According to the simple calculation, it is shown that the redundancy of ramification structure yields high fracture toughness.

Secondly, the quasi-static crack propagation is studied in bulk materials. The small scale yielding condition is assumed and the linear elastic solution specifies the boundary displacement component. The boundary value problem in linear elasticity is solved for increasing remote stress intensity factor by using finite element method. The displacement field and stress distribution obtained by the simulation is discussed to study the mechanism of crack propagation. The relationships between the remote stress intensity factor and representative crack length are plotted for several cases of different microstructures. The effective interface area and the effective surface energy depends on the internal microstructure of interface. The effect of geometry cause the complex pattern of bonding-debonding domain. As the result, the representative length scale of fracture process zone depends on the heterogeneity and morphology of microscopic structure. The fracture toughness which is estimated as a remote stress intensity factor changes associated with the change of the fracture process zone due to the microstructure.

2. Theory

2.1. Cohesive Zone Model

Cohesive zone model is frequently used to analyze crack propagation. In this modeling, a cohesive zone is placed between bulk elements as shown in Fig.1. Fracture can be regarded as elements separating along the cohesive surface resisted by cohesive traction[2][3]. As the separation occurs, the traction increases to a maximum and then falls back to 0. The procedure means the element separates completely, and the area under the traction-separation curve corresponds with the effective surface energy that needed for complete separation.

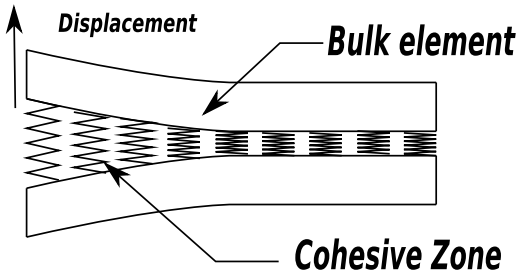

Figure 1. Cohesive zone model placed between bulk elements

2.2. Cohesive Zone Law

The traction vector $\boldsymbol{T} = (T_n, T_t)$ can be derived from the effective surface energy $\phi(\boldsymbol{\Delta})$.(*E.g.*[4][5])

$$\boldsymbol{T} = -\frac{\partial\phi(\boldsymbol{\Delta})}{\partial(\boldsymbol{\Delta})} \tag{1}$$

where $\boldsymbol{\Delta} = (\Delta_n, \Delta_t)$. The components T_n, T_t and Δ_n, Δ_t are the normal and tangential components of traction vector and relative displacement vector, respectively.

The surface energy [4] can be written as:

$$\phi(\Delta_n, \Delta_t) = \phi_n + \phi_n \exp\left(-\frac{\Delta_n}{\delta_n}\right)\left(\left[1 - r + \frac{\Delta_n}{\delta_n}\right]\frac{1-q}{r-1} - \left[q + \left(\frac{r-q}{r-1}\right)\frac{\Delta_n}{\delta_n}\right]\exp\left(-\frac{\Delta_t^2}{\delta_t^2}\right)\right) \tag{2}$$

where δ_n and δ_t represent the character length that satisfy $T_n(\delta_n) = \sigma_{\max}$, $T_t(\delta_t/\sqrt{2}) = \tau_{\max}$. Stress $\sigma_{\max}$ and $\tau_{\max}$ represent the maximum of normal traction and tangential traction, respectively. Pameters are defined as $q = \phi_t/\phi_n$, $r = \Delta_n'/\delta_n$, where Δ_n' represents the value of Δ_n when $T_n = 0$. ϕ_n and ϕ_t are the areas under the normal traction-separation curve and the shear traction-separation curve representing the surface energy for complete separation respectively and can be calculated as:

$$\phi_n = \sigma_{\max}\exp(1)\delta_n, \quad \phi_t = \sqrt{\exp(1)/2}\tau_{\max}\delta_t \tag{3}$$

From Eqs.(1) and (2),the normal and shear traction can be obtained:

$$T_n = \frac{\phi_n}{\delta_n}\exp\left(-\frac{\Delta_n}{\delta_n}\right)\left(\frac{\Delta_n}{\delta_n}\exp\left(-\frac{\Delta_n^2}{\delta_n^2}\right) + \frac{1-q}{r-1}\left[1 - \exp(-\frac{\Delta_n^2}{\delta_n^2})\right]\left[r - \frac{\Delta_n}{\delta_n}\right]\right) \tag{4}$$

$$T_t = 2\left(\frac{\phi_n \Delta_t}{\delta_t^2}\right)\left[q + \left(\frac{r-q}{r-1}\right)\frac{\Delta_n}{\delta_n}\right]\exp\left(-\frac{\Delta_n}{\delta_n}\right)\exp\left(-\frac{\Delta_t^2}{\delta_t^2}\right) \tag{5}$$

2.3. Frame element

Frame element is the combination of truss element which represents axial tension and beam element that represents bending (E.g. [6]). Consider the frame element shown in Fig. 2, the element nodal

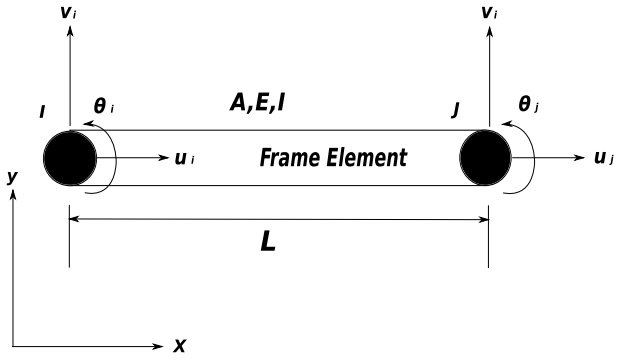

Figure 2. Image of frame element

displacement vector $\boldsymbol{d}_{\text{Frame}}$ and the vector of element nodal loads $\boldsymbol{F}_{\text{Frame}}$ are set as:

$$\left(\ \boldsymbol{d}_{\text{Frame}}\ \right)^{\text{T}} = \left(\ u_i \quad v_i \quad \theta_i \quad u_j \quad v_j \quad \theta_j\ \right)^{\text{T}} \tag{6}$$

$$\left(\ \boldsymbol{F}_{\text{Frame}}\ \right)^{\text{T}} = \left(\ P_i \quad Q_i \quad M_i \quad P_j \quad Q_j \quad M_j\ \right)^{\text{T}} \tag{7}$$

As shown in Fig. 2, u, v, and θ are the x-direction displacement, y-direction displacement and deflection angle, respectively. P, Q, and M represent the x-direction load, y-direction load and bending moment, respectively. The stiff equation of frame element can be expressed as:

$$\left(\ F_{\text{Frame}}\ \right) = \left(\ k_{\text{Frame}}\ \right)\left(\ d_{\text{Frame}}\ \right) \tag{8}$$

where $[k_{\text{Frame}}]$ represents the element stiff matrix of the frame element of x-direction. Furthermore, if we set the length, area of cross section, Young's modulus and moment of inertial of area as l, A, E, I, then consider the frame element that inclined at the degree of β to the x-direction.

By coordinate transformation, the stiff equation of the frame element of any direction can be obtained:

$$\begin{pmatrix} P_i^* \\ Q_i^* \\ M_i^* \\ P_j^* \\ Q_j^* \\ M_j^* \end{pmatrix} = \begin{bmatrix} F & G & H & -F & -G & H \\ G & U & V & -G & -U & V \\ H & V & S & -H & -V & T \\ -F & -G & -H & F & G & -H \\ -G & -U & -V & G & U & -V \\ H & V & T & -H & -V & S \end{bmatrix} \begin{pmatrix} u_i^* \\ v_i^* \\ \theta_i^* \\ u_j^* \\ v_j^* \\ \theta_j^* \end{pmatrix} \tag{9}$$

Where the components can be represented as:

$$
\begin{aligned}
S &= \frac{4EI}{l} \\
T &= \frac{2EI}{l} \\
F &= \frac{AE}{l}\cos^2\beta + \frac{12EI}{l^3}\sin^2\beta \\
G &= \frac{AE}{l}\sin\beta\cos\beta - \frac{12EI}{l^3}\sin\beta\cos\beta \\
H &= -\frac{6EI}{l^2}\sin\beta \\
U &= \frac{AE}{l}\sin^2\beta + \frac{12EI}{l^3}\cos^2\beta \\
V &= \frac{6EI}{l^2}\cos\beta
\end{aligned}
$$

2.4. Energy Release Rate

With the propagation of crack, it is found the surface energy decreases to form new crack surface. Using the stress intensity factor K_I, the potential energy release rate $\mathcal{G}$ can be calculated as:

$$\mathcal{G} = \frac{1-\nu^2}{E}K_I^2. \tag{10}$$

When considering about double cantilever beam, with the Young's modulus of E,and the moment of inertial of area as I, and the bending moment M acting on the free edge of the beam, the energy release rate can be calculated as:

$$\mathcal{G} = \frac{M^2}{2EI} \tag{11}$$

3. Analysis Model and Analysis method

3.1. Discrete Cohesive Zone Model

Consider a linear elastic solid in Fig. 3 with Young's modulus of E and Poisson's ratio of ν and established with cohesive zone model in Fig. 4(a). Fig. 4(b) shows the general continuously cohesive zone model, while Fig. 4(c) is the discrete cohesive zone model on the basis of Fig. 4(b) with periodic characteristic length of l. In the periodic structure, set the cohesive zone model with the length of b,and make the last $l-b$ of debonding area. Also in this study, we set $b = 1/2l$. The small scale yielding condition is assumed and the boundary condition is set with a displacement field of $K_{\mathrm{I}} = \dot{K}_{\mathrm{I}}t$ with $\dot{K}_{\mathrm{I}} = 50\mathrm{GPa}\sqrt{\mathrm{m}}/\mathrm{s}$. Using the discrete cohesive model,crack propagation is studied.

With the Griffith theory, fracture toughness K_{IC} can be evaluated with surface energy Γ as:

$$K_{\mathrm{IC}} = \sqrt{\frac{E\Gamma}{1-\nu^2}} \tag{12}$$

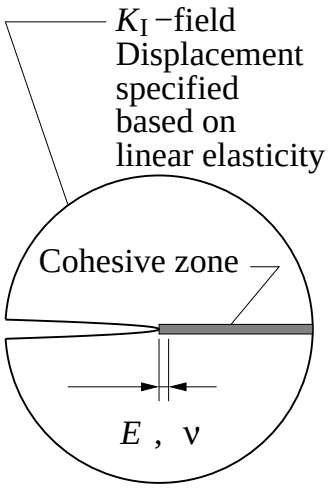

Figure 3. Schematics of problem

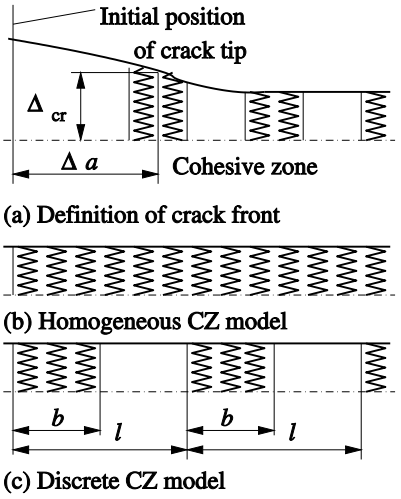

Figure 4. Detail of Cohesive zone

And here for general continuously cohesive zone model, $\Gamma = \phi_n$. So with $b = 1/2l$, the discrete cohesive zone model has the surface energy of $1/2\phi_n$ and the stress intensity factor can be obtained as $K_I = \sqrt{1/2}K_{IC}$.

3.2. Microscopic Structure with Cohesive Zone Model

Microscopic structures with different mythologies show unique feature of strength. Consider two patterns of structures made of frame elements bound with cohesive zone shown in Fig.5 and Fig.6, set the y-direction displacement and simulate the separation of the element.

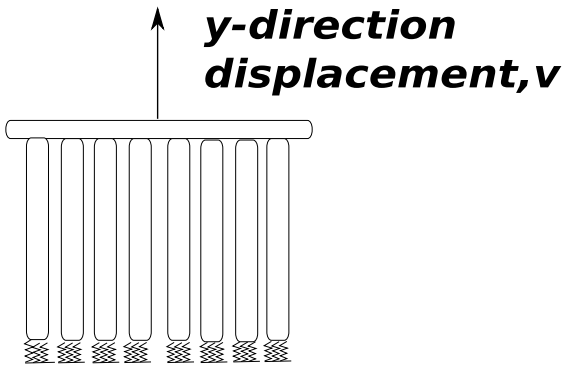

Figure 5. Unit Discrete Structure

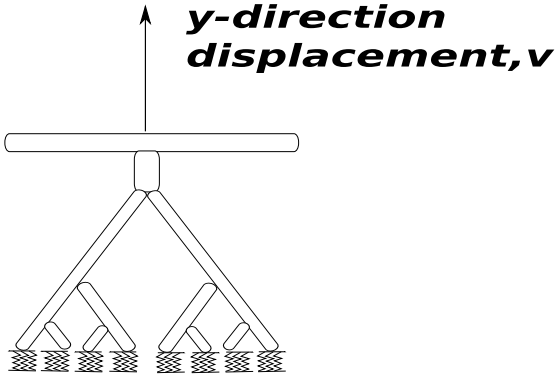

Figure 6. Unit Hierarchical Structure

The bottom of the structures are bound with cohesive zone model, when separation happens, the traction-time curve can be shown as Fig.7

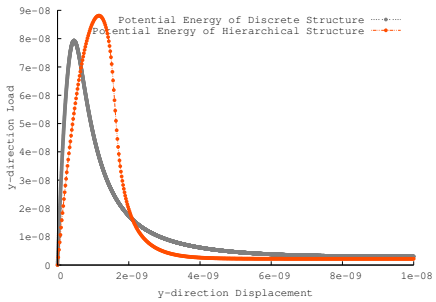

Figure 7. Force-displacement relations of microsopic structures

With the feature talked above, by using the model of continuous cohesive zone model, continuous microscopic structures can be obtained. As shown in Fig. 8, cohesive zone is replaced by structures. All the structures are binding with cohesive zone models at the end of the elements, and the angular velocity at the free edge is set as $\omega = 5 \times 10^{-7}$rads/s.

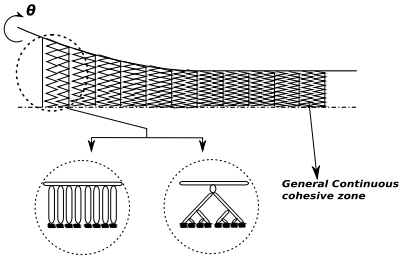

(a) Continuous Structure with cohesive zone model

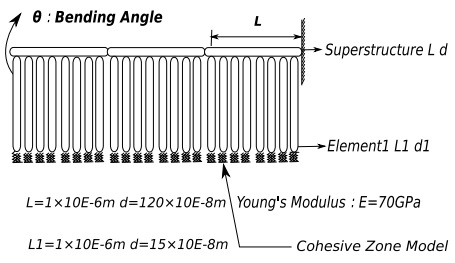

(b) Discrete Structure with cohesive zone model

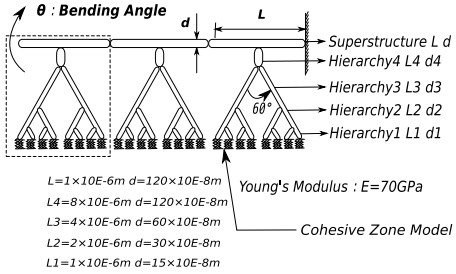

(c) Hierarchical ramification structure with cohesive zone model

Figure 8. Schematics of pealing problem of canti-lever

4. Analysis Result

4.1. Discrete Cohesive Model

The fracture toughness of the general continuously cohesive zone model can be calculated as $K^*_{\mathrm{IC}} = 0.358\mathrm{MPa}\sqrt{\mathrm{m}}$, therefor the theoretical value of the stress intensity factor will be $K_{\mathrm{IC}} = \sqrt{1/2}K^*_{\mathrm{IC}}$.

Using discrete cohesive zone model and general continuously cohesive zone model to simulate the crack propagation and comparing the stress intensity factor as shown in Fig.9

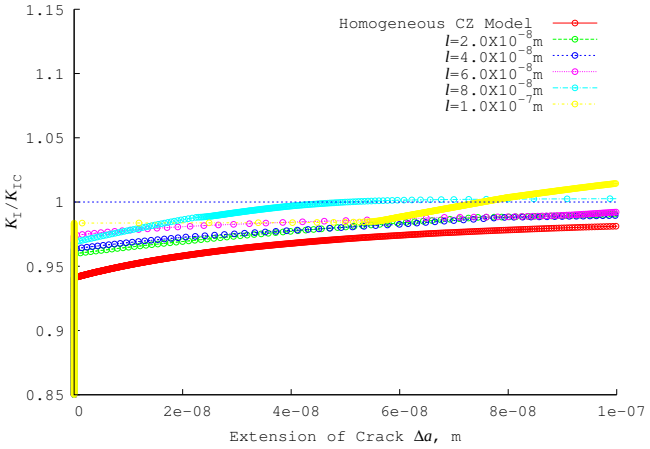

Figure 9. The stress intensity factor of discrete cohesive zone model of different characteristic lengths comparing with the theoretical value

Figure 9 shows the result of different characteristic lengths. The strength of the material increases with the characteristic length. Also, the stress intensity factors of discrete cohesive zone models are all above the one of general continuously cohesive zone model. Therefore, the possibility that the interface morphology of cohesive zone has an impact on the strength of material is illustrated.

4.2. Microscopic Structure with cohesive zone model

The average potential energy to make a new fracture surface can be calculated as $\phi_n^* = \phi_n/\Delta d = 1.28 \times 10^{-10}$J/m. Using this data, the theoretical moment in proportion to strength of the bulk material can be obtained as $K^* = \sqrt{\phi_n^* EI} = 9.55 \times 10^{-13}$Nm.

By using simulation, the simulate data of the strength of structures with cohesive zone model and the deformation can be obtained.

As shown in Fig.10, the strength of discrete structure exceeds the one of hierarchical structure at first and is reversed during the crack propagation . When crack propagates, the strength of discrete structure turns constant while the one of hierarchical structure shows several jump which represents the thorough separation of unit structures. Although theoretical result overwhelms simulation results, since the result of hierarchical structure increases during element separation, the strength of hierarchical structure shows more resistance to crack propagation.

When the strength of hierarchical structure jumps as shown in Fig.12, crack propagation occurs. From the deformed hierarchical structure graph, the details of crack propagation can be illustrated.

Figures 13(a)- (h) show the details of crack propagation and element separation. The upper graphs represent the total image of deformed structures while the lower ones represent the enlarged view

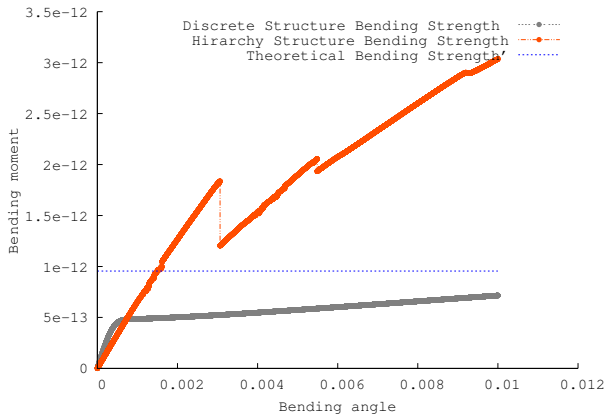

Figure 10. Strength of different models

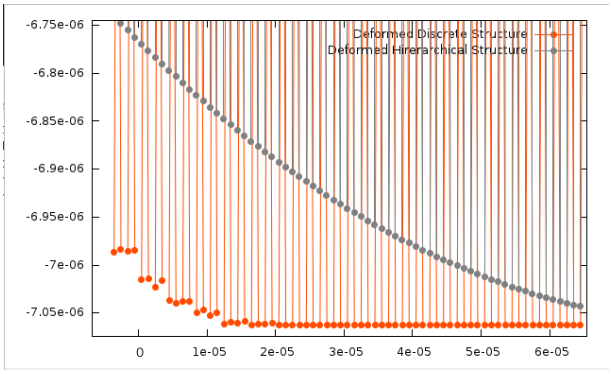

Figure 11. Deformed Microscopic Structures

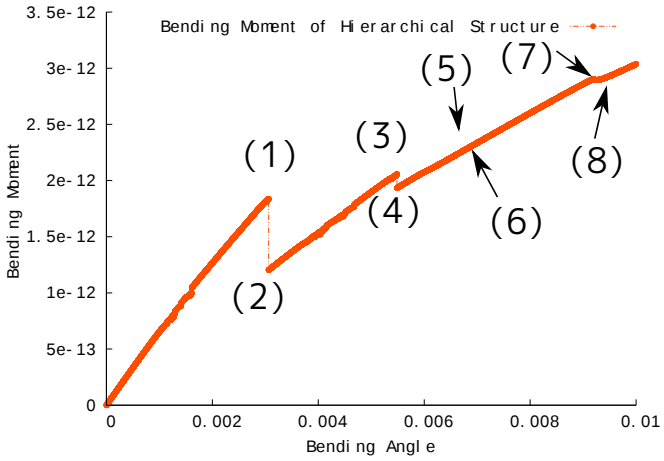

Figure 12. Separations on cohesive zone during crack propagation

of the cohesive zone. When first jump happens in Fig.12 at (1) and (2), the first unit hierarchical structure separates completely and crack propagates as in Fig. 13(a) and Fig. 13(b). The second jump at (3) and (4) corresponds to Fig. 13(c) and Fig. 13(d), half of the unit structure separates while the other half parts contains both bonding and separated elements. This half parts completely separates at (5) and (6) shows in Fig12 without jumps.After the first two unit structures separate completely, the third one begin to separates at (7) and at (8) half of the unit structure thoroughly separates.

The hierarchical structure separates at a certain distributive way. Due to the special feature of hierarchical structure, the elements do not separate in regular order. Instead, after the initial separation, the element separates next shifts in one structure.

After all the elements separate in one structure, the crack propagation happens. While for discrete structure, the elements separate in the regular order, after the first separation happens, the elements next separates sequentially. Discrete structure may be destroyed quickly after the first element separation, while hierarchical structure can suffer more due to its special separating feature.

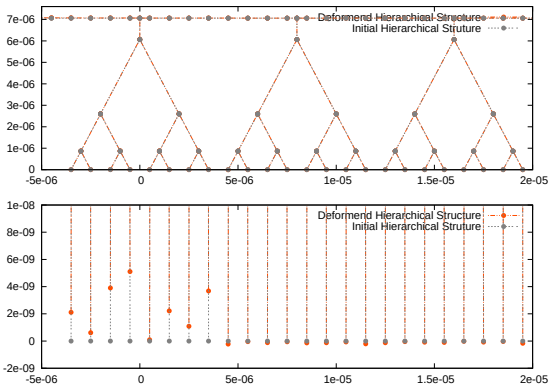

(a) at point(1)

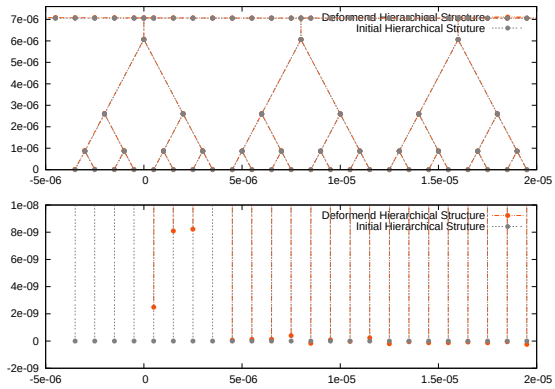

(b) at point(2)

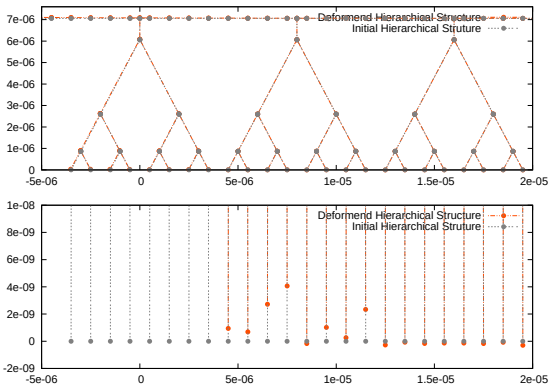

(c) at point(3)

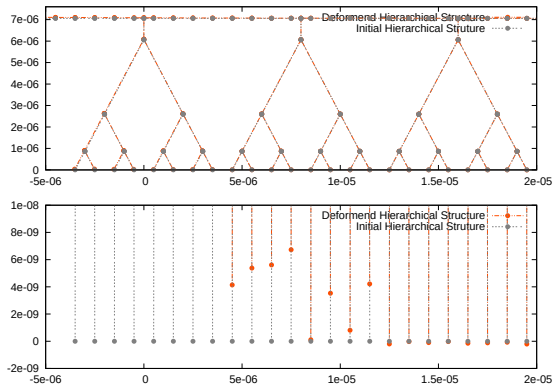

(d) at point(4)

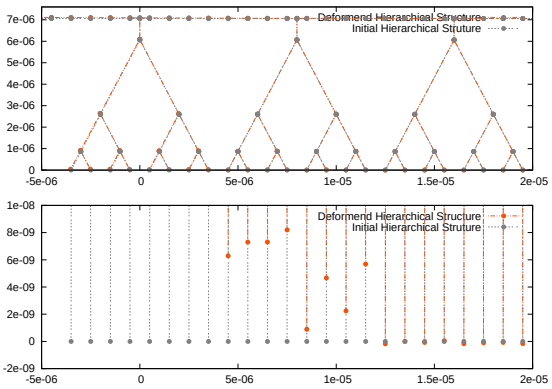

(e) at point(5)

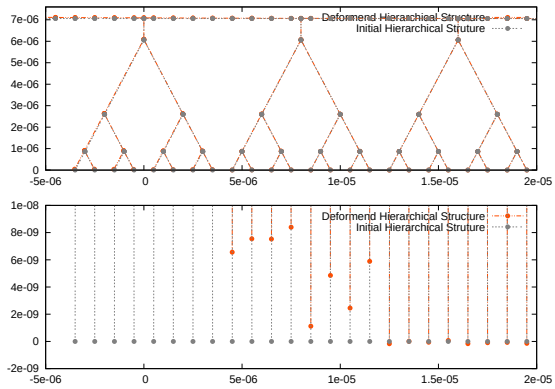

(f) at point(6)

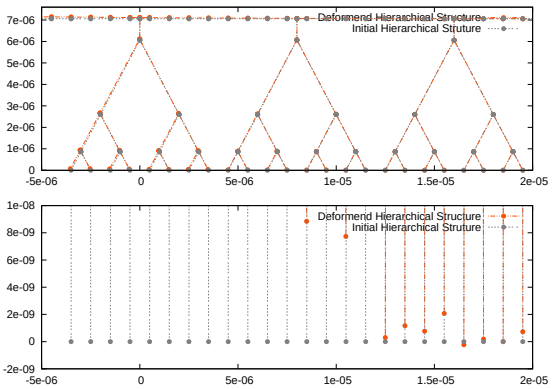

(g) at point(7)

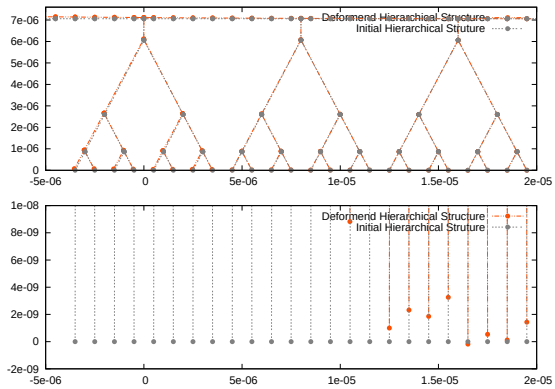

(h) at point(8)

Figure 13. Deformed Hierarchical Structure

5. Conclusions

The strength of the material has been evaluated via simulation of discrete cohesive zone model and microscopic structures bound with cohesive zone model. By changing the morphology of the interface, sophisticated design of the strength and the properties of crack propagation of material will be possible.

Acknowledgments

This work was supported by Grants-in-Aid for Scientific Research (KAKENHI). We would also like to thank Prof. Y. Doi whose opinions have helped us very much throughout the production of this study.

References

[1] D. Xie, A.G. Salvi, A.M. Waas, A.Caliskan, Discrete Cohesive Zone Model to Simulate Static Fracture in Carbon Fiber Textile Composites, AIAA2005-2320 (2005) 1-21.
[2] René Kregting, Cohesive zone model towards a robust implementation of irreversible behaviour, MT05.11, 2005.
[3] P. D. Zavattieri, L.G. Hector Jr, A.F. Bower, Cohesive zone simulations of crack growth along a rough interface between two elastic-plastic solids, Eng Fract Mech, 75 (2008) 4309-4332.
[4] X.-P. Xu, A. Needleman, Void nucleation by inclusion debonding in a crystal matrix, Model Simul Mat Sci Eng, 1 (1992) 111-132.
[5] A. Nakatani, W.J. Drugan, E. Van der Giessen and A. Needleman,Crack tip fields at a ductile single crystal-rigid material interface, Int J Fract, 122 (2003) 131-159.
[6] R.D.Cook, Concepts and Applications of Finite Element Analysis, Wiley, 1981, pp.56-89.